Wavelet Regularization and the Continuous Relaxation Spectrum.

A.R. Davies[a,*], N.J. Goulding[a]

[a]*School of Mathematics, Cardiff University, Senghennydd Road, Cardiff CF24 4AG, UK.*

Abstract

The purpose of this paper is to show how continuous wavelet analysis can be used to establish natural models for the continuous relaxation spectrum of a polymeric material. A method of wavelet regularization is proposed for the practical recovery of the continuous spectrum over a limited range of relaxation times. Working with logarithmic variables (log-frequency and log-time), it may be seen that the loss modulus is a scaling function transform of the continuous relaxation spectrum. It is shown how the decomposition formula of Calderón and Mallat may be used to reconstruct the spectrum from measurements of storage and loss moduli. At practical levels of resolution, the spectrum may be represented as a finite sum of hyperbolic scaling functions. There are two principal regularization mechanisms, namely, *sparsity* (the number of terms in the sum), and *scale* (which controls both resolution and smoothness). The method of wavelet regularization is illustrated by recovering spectra from both synthetic and real data.

Keywords: continuous wavelet transform, regularization, wavelet dictionaries, continuous relaxation spectrum, sparse approximation, resolution.

1. Introduction

In an incompressible shear deformation, Boltzmann's general linear integral model for viscoelastic materials [1] relates the stress $\sigma(t)$ to the strain-rate $\dot{\gamma}(t)$ in the form

$$\sigma(t) = \int_{-\infty}^{t} G(t-t')\dot{\gamma}(t')dt', \tag{1.1}$$

where $G(t)$ is a monotonically decreasing relaxation function. In keeping with the principle of fading memory [2], the memory function is also monotonically decreasing, which means that the first derivative $\frac{dG}{dt}$ is monotonically increasing. Bernstein's theorem [3] states that successive derivatives of $G(t)$ of all orders

*Corresponding author. Electronic mail: DaviesR@cardiff.ac.uk

are alternately monotonically increasing and decreasing if and only if $G(t)$ is the Laplace transform of a positive measure. Under this constraint $G(t)$ is said to be *completely monotone* and may be written in the form

$$G(t) = G_e + \int_0^\infty H(\tau) e^{-\frac{t}{\tau}} \frac{d\tau}{\tau}, \tag{1.2}$$

where G_e is a material constant, given by

$$G_e = \lim_{t \to \infty} G(t), \tag{1.3}$$

and $H(\tau)$ is an un-normalized non-negative density function associated with a continuous range of relaxation times τ. In a generalized Maxwell model $H(\tau)d\tau$ may be thought of as the viscosity associated with a Maxwell element with relaxation times between τ and $\tau + d\tau$. Equation (1.2) serves as a mathematical definition of the continuous relaxation spectrum, $H(\tau)$. The total viscosity η of the material is then given by

$$\eta = \int_0^\infty H(\tau) d\tau < \infty. \tag{1.4}$$

In an oscillatory shear experiment [4,5], an applied strain

$$\gamma(t) = \begin{cases} \gamma_0 e^{i\omega t} & \text{if } t \geq 0; \\ 0 & \text{if } t < 0, \end{cases} \tag{1.5}$$

with constant angular frequency ω enables equation (1.1) to be written in the form

$$\sigma(t) = G^*(\omega)\gamma(t), \tag{1.6}$$

where $G^*(\omega)$ is a complex shear modulus given by

$$G^*(\omega) = G_e + i\omega \int_0^\infty [G(t') - G_e] e^{-i\omega t'} dt'. \tag{1.7}$$

Under the transformation $z = i\omega^{-1}$ it follows from equation (1.7) that $G^*(\omega)$ is related to the continuous relaxation spectrum by the following complex Steiltjes transforms

$$G^*(\omega) = G_e + \int_0^\infty \frac{i\omega}{1 + i\omega\tau} H(\tau) d\tau = G_e + \int_0^\infty \frac{H(\tau)}{\tau - z} d\tau. \tag{1.8}$$

If $G^*(\omega)$ were measurable at all frequencies $0 < \omega < \infty$, then in principle the transform (1.8) can be inverted to yield the spectrum for all relaxation times $0 < \tau < \infty$. The oscillatory shear experiment, however, can be repeated only for a limited range of sampled frequencies, which means that exact inversion formulae based on semi-infinite intervals become problematic. Furthermore, when z is pure imaginary, as is the case in equation (1.8), then recovering

the spectrum from the complex modulus is an exponentially ill-posed inverse problem, and is highly unstable to small perturbations in the data.

Splitting $G^*(\omega)$ into its real and imaginary parts, the storage and loss moduli are given by the pair of Fredholm integral equations

$$G'(\omega) = G_e + \int_0^\infty \frac{\omega^2\tau^2}{1+\omega^2\tau^2} H(\tau)\frac{d\tau}{\tau} \tag{1.9}$$

$$G''(\omega) = \int_0^\infty \frac{\omega\tau}{1+\omega^2\tau^2} H(\tau)\frac{d\tau}{\tau}. \tag{1.10}$$

The sampling localization algorithm [6] based on the exact inversion formula

$$H(\tau) = \lim_{\epsilon\to 0}\int_{-\infty}^{\infty}\int_{-\infty}^{\infty} G''(\omega)\cosh\left(\frac{\pi}{2}p\right) e^{-\frac{1}{2}\epsilon^2 p^2} e^{ip\ln(\omega\tau)} dp\, d\ln\omega \tag{1.11}$$

shows that it is not necessary to have knowledge of the complex modulus at all frequencies in order to determine the spectrum in a limited time range. In particular, if the storage and loss moduli are given for a limited range of frequencies, $\omega_{\min} < \omega < \omega_{\max}$, say, then (1.11) determines the spectrum in the reduced reciprocal range of relaxation times $\omega_{\max}^{-1}e^{\pi/2} < \tau < \omega_{\min}^{-1}e^{-\pi/2}$. Renardy [7] points out that since G' and G'' are real analytic functions, then if they are known in a finite interval, in principle they are immediately determined for all positive frequencies by analytic continuation. However, Renardy also points out that this observation is of limited value since no practical algorithm exists for performing the analytic continuation to any acceptable degree of accuracy.

In this paper we will set the constant G_e to zero. This is the relevant case for viscoelastic liquids. The case for viscoelastic solids, with $G_e > 0$, can be treated by means of a slight modification of the theory.

It is an inherent premise in the Boltzmann formulation of linear viscoelasticity that, for shear deformations at fixed temperature and pressure, every material has a *unique* continuous relaxation spectrum. This is not the case for *discrete spectra* of the form

$$H(\tau) = \sum_n \eta_n \delta(\tau - \tau_n). \tag{1.12}$$

Methods for determining discrete spectra include the use of nonlinear regression [8,9], Tikhonov regularisation [10], maximum entropy regularisation [11], sampling localisation [12,13] and Prony series [14]. Different methods can give rise to different discrete spectra. There is no *unique* discrete spectrum for any given material. Malkin [15] states that: "*The discrete relaxation spectrum is just a convenient way of representing experimental data... It has no basic physical meaning*". Chow and Zukoski [16,17] state: "*No line spectrum - produced by whatever method - is ever the true spectrum*". Dealy and Larson [18] also outline certain disadvantages in working with discrete spectra.

Previous work in approximating continuous spectra has relied exclusively on parametric curve fitting models. We cite Winter [19], Anderssen [20] (who

advocates Kohlrausch (stretched exponential) functions), Bailly & Stadler [21], Stadler [22] (who advocate piecewise cubic Hermite splines) and Malkin [23]. There is no theoretical foundation for relating these empirical models directly to the mathematical theory of linear viscoelasticity. The aim of this paper is to show that wavelet analysis establishes natural models for the continuous relaxation spectrum. In particular, we show that there exist scaling function transforms which are intrinsic to the theory of linear viscoelasticity, which give rise to natural representations for the continuous spectrum.

The paper is structured as follows. In §2 we establish a link between continuous wavelet transforms and the theory of linear viscoelasticity. In particular, we prove that the error term in the approximation due to Fuoss and Kirkwood for the continuous relaxation function is a wavelet. This enables us to devise, in §3, an approximation and regularization strategy for the continuous spectrum. This is based on the decomposition formula due to Calderón and Mallat. *Scale* and *sparsity* are presented as regularization parameters, and resolution is analyzed in terms of effective bandwidths. Transformed dictionaries which provide new bases for representing storage and loss moduli are introduced in §4, together with a basic search algorithm for selecting terms from the dictionary to fit the dynamic data. Continuous spectra recovered by the method of wavelet regularization from both synthetic and real data are discussed in §5. The use of *minimum total curvature* as a selection criterion for choosing the scale of the approximation is demonstrated. Conclusions are drawn in §6.

2. Wavelet Transforms in the Theory of Linear Viscoelasticity

2.1. The storage and loss moduli in convolution form

Using the substitutions

$$H(\tau) = h(t), \quad G'(\omega) = \tfrac{1}{2} g_1(x), \quad G''(\omega) = \tfrac{1}{2} g_2(x) \tag{2.1}$$

$$\text{where} \quad x = \ln \omega \quad \text{and} \quad t = -\ln \tau, \tag{2.2}$$

the real and imaginary parts of (1.8) may be written in convolution form as

$$g_1(x) = [1 + \tanh(x)] \star h(x) \tag{2.3}$$

$$g_2(x) = \operatorname{sech}(x) \star h(x), \tag{2.4}$$

where $\star$ denotes convolution, i.e.

$$(f \star g)(x) = \int_{-\infty}^{\infty} f(x-s) g(s) ds. \tag{2.5}$$

We will assume throughout this article that $h(x) \in L^2(\mathbb{R})$, which implies that its Fourier transform $\widehat{h}(p)$ exists. Throughout the paper we use the following convention for the Fourier transform

$$\widehat{h}(p) = \int_{-\infty}^{\infty} h(t) e^{-ipt} dt. \tag{2.6}$$

Since the Fourier transform of sech(x) is $\pi\text{sech}\left(\frac{\pi}{2}p\right)$, it follows from the convolution theorem for Fourier transforms that

$$\widehat{g_2}(p) \quad = \quad \pi\text{sech}\left(\frac{\pi}{2}p\right)\widehat{h}(p). \tag{2.7}$$

Inverting equation (2.7), we obtain

$$\widehat{h}(p) \quad = \quad \frac{1}{\pi}\cosh\left(\frac{\pi}{2}p\right)\widehat{g_2}(p). \tag{2.8}$$

Our assumption that $h(x) \in L^2(\mathbb{R})$ means that $\widehat{g_2}(p)$ must tend to zero faster than $\text{sech}\left(\frac{\pi}{2}p\right)$ as $|p| \to \infty$. The factor multiplying $\widehat{g_2}(p)$ in (2.8) has exponential growth (with index $\frac{\pi}{2}$) as $|p| \to \infty$. Any noise present in g_2 will have its Fourier transform amplified by a factor $e^{\frac{\pi}{2}|p|}$ as $|p| \to \infty$, which proves that the problem of determining the continuous relaxation spectrum from the loss modulus is exponentially ill-posed with index $\frac{\pi}{2}$.

Equations (1.9) and (1.10), and their logarithmic counterparts (2.3) and (2.4), are intimately linked to continuous wavelet transforms, where the wavelets are constructed from simple hyperbolic functions. This link is established by a study of the term, $E(\tau)$, in the equation

$$H(\tau) \quad = \quad \frac{2}{\pi}G''\left(\tau^{-1}\right) + E(\tau). \tag{2.9}$$

Ferry [24] attributes the approximation

$$H(\tau) \approx \frac{2}{\pi}G''\left(\tau^{-1}\right) \tag{2.10}$$

to Fuoss and Kirkwood [25]. We shall show that the correction term $E(\tau)$ is a wavelet.

2.2. Wavelets and continuous wavelet transforms

A wavelet is a function in the shape of a small wave with zero area. In Fig. 1, a wavelet $\psi(x)$ is shown, together with its scaling function $\phi(x)$ which we define below. We shall be concerned with two classes of wavelets, Ω and Ω^+. Ω will consist of real-valued functions $\psi \in L^2(\mathbb{R})$ with the following properties

$$\text{(i)} \quad \psi(x) = \psi(-x), \quad (\psi \text{ is even}); \tag{2.11}$$

$$\text{(ii)} \quad \int_{-\infty}^{\infty}\psi(x)dx = 0, \quad (\text{the graph of } \psi \text{ has zero area}); \tag{2.12}$$

(iii) there exists a constant C_ψ such that

$$0 < C_\psi = \int_0^\infty \frac{|\widehat{\psi}(p)|^2}{p}dp < \infty. \tag{2.13}$$

Under the constraints (2.11)-(2.13), for each $\psi \in \Omega$, there exists a unique real valued *scaling function* $\phi \in L^2(\mathbb{R})$ whose Fourier transform is defined by

$$\widehat{\phi}(p) = \left[\int_p^\infty \frac{|\widehat{\psi}(\xi)|^2}{\xi}d\xi\right]^{\frac{1}{2}} \tag{2.14}$$

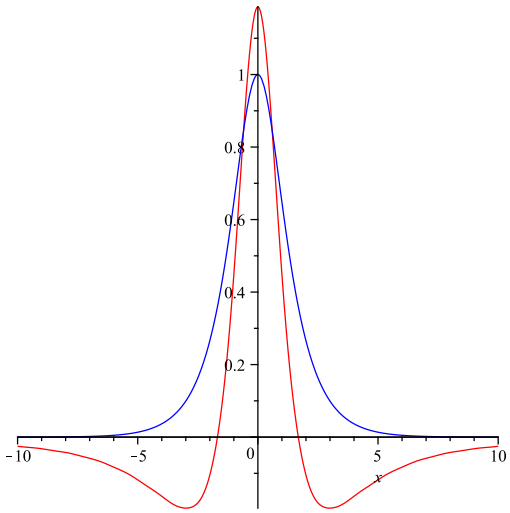

Figure 1: A wavelet $\psi(x)$ (—) and its corresponding scaling function $\phi(x)$ (—).

and which has non-zero area given by

$$\widehat{\phi}(0) = (C_\psi)^{\frac{1}{2}} . \tag{2.15}$$

ψ is sometimes called a *mother wavelet* with corresponding *father wavelet* ϕ. If $\psi \in \Omega$ then it is easily shown that

$$\text{(iv)} \quad \phi \text{ is an even function;} \tag{2.16}$$

$$\text{(v)} \quad \psi \star \psi \in \Omega, \quad \text{(the autoconvolution is a wavelet);} \tag{2.17}$$

$$\text{(vi)} \quad (\psi \star \psi)(x) = \frac{d}{dx}[x(\phi \star \phi)(x)]; \tag{2.18}$$

$$\text{(vi)} \quad (\phi \star \phi)(x) = \int_{-\infty}^{\infty} \left\{ \int_1^{\infty} \psi\left(\frac{t}{s}\right) \psi\left(\frac{x-t}{s}\right) \frac{ds}{s^3} \right\} dt. \tag{2.19}$$

Equation (2.19) shows that the scaling function is a function made up of all wavelet scales $s \geq 1$.

The wavelet class Ω^+ extends Ω to include real-valued wavelets that are not even. $\psi \in L^2(\mathbb{R})$ is in Ω^+ if properties (2.12) and (2.13) are satisfied. In Ω, ψ is real-valued and even, and its Fourier transform $\hat{\psi}$ is real-valued. In Ω^+, ψ is real-valued, but need not be even, and so $\hat{\psi}$ can be complex-valued.

The *continuous wavelet transform* of $h \in L^2(\mathbb{R})$ at the frequency x and scale s is defined by the convolution product

$$[Wh](s,x) = (h \star \psi_s)(x), \tag{2.20}$$

$$\text{where} \quad \psi_s(x) = \frac{1}{\sqrt{s}} \psi\left(\frac{x}{s}\right), \quad \psi \in \Omega, \ s > 0. \tag{2.21}$$

The wavelet transform $[Wh](s,x)$ localizes the function $h(t)$ in the vicinity of $t=x$. In particular, when $0<s<1$, a peak in $h(t)$ at $t=x$ will be sharpened by the transform $[Wh](s,x)$. The smaller the scale s the more pronounced the sharpening of the peak will be.

The corresponding *scaling function transform* of $h \in L^2(\mathbb{R})$ is given by

$$[Vh](s,x) \quad = \quad (h \star \phi_s)(x), \tag{2.22}$$

where

$$\phi_s(x) = \frac{1}{\sqrt{s}}\phi\left(\frac{x}{s}\right), \quad s>0. \tag{2.23}$$

The scaling function transform behaves in a totally different way to the wavelet transform, since $[Vh](s,x)$ is a low-pass filter applied to h. Whatever the value of $s>0$, a peak in $h(t)$ at $t=x$ will be broadened by the transform. The larger the value of s the more pronounced the broadening of the peak will be.

Equation (2.4) shows that in terms of log-frequency, the loss modulus $g_2(x)$ is a *scaling function transform* of the continuous relaxation spectrum, at unit scaling $s=1$, i.e.

$$g_2(x) = [Vh](1,x) = (h \star \phi)(x) \tag{2.24}$$

with

$$\phi(x) = \phi_1(x) = \operatorname{sech}(x) = \operatorname{sech}(\ln \omega). \tag{2.25}$$

It is possible to quantify the amount of broadening induced by the transform (2.24). Let $\hat{h}(p)$ decay exponentially like $\operatorname{sech}\left(\frac{1}{2}\sigma\pi p\right)$ as $p \to \pm\infty$, where $\sigma>0$. Then, from the convolution theorem for Fourier transforms, $\hat{g_2}(p)$ decays like $\operatorname{sech}\left[\frac{1}{2}(\sigma+1)\pi p\right]$ as $p \to \pm\infty$. This means that if $h(t)$ has a peak of scale σ at $t=t_0$, then $g_2(x)$ has a peak of scale $\sigma+1$ at $x=t_0$. The problem of recovering the spectrum from the loss modulus can therefore be viewed as a problem in reduction of scale of the loss modulus.

Equation (2.24) is a fundamental observation which motivates the main results of this paper. The scaling function $\phi(x) = \operatorname{sech}(x)$ and its associated mother wavelet $\psi(x)$ are plotted together in Fig. 1. $\psi(x)$ has been calculated numerically since it cannot be expressed in closed form.

2.3. Calderón-Mallat decomposition and the link with linear viscoelasticity

Let $(\tilde{\psi},\tilde{\phi})$ be an arbitrary mother-father wavelet pair with $\tilde{\psi} \in \Omega$. Following an original theorem of Calderón [26], Mallat [27] has shown that any real-valued function $h \in L^2(\mathbb{R})$ can be represented as follows

$$h(t) \quad = \quad \frac{1}{C_{\tilde{\psi}}}\int_0^{\sigma}\left(h \star \tilde{\psi}_s \star \tilde{\psi}_s\right)(t)\,\frac{ds}{s^2} + \frac{1}{C_{\tilde{\psi}}\sigma}(h \star \tilde{\phi}_\sigma \star \tilde{\phi}_\sigma)(t). \tag{2.26}$$

We shall refer to equation (2.26) as the Calderón-Mallat decomposition of h. It is customary to think of (2.26) as an inversion formula for h in terms of

the wavelet transforms $h \star \tilde{\psi}_s$ over the range of scales $0 < s \leq \sigma$, and the single scaling function transform $h \star \tilde{\phi}_\sigma$. The first (integral) term in (2.26) is a projection of h into a subspace of $L^2(\mathbb{R})$. When σ is small this term represents the high resolution components of h. The second term in (2.26) constitutes a low-pass filter applied to h. It belongs to the complementary subspace of $L^2(\mathbb{R})$ and incorporates the sum of (lower resolution) components over the remaining scales $s \geq \sigma$.

In this paper we use the Calderón-Mallat decomposition (2.26) in a different way from the customary approach outlined above. First, we regularize the inversion by omitting small scales (high resolution terms) from (2.26). We then use the remaining terms as a model for the continuous relaxation spectrum, at a chosen scale σ. In this sense the scale σ acts as a regularization parameter.

Let $\psi^\star = \tilde{\psi} \star \tilde{\psi}$ and $\phi = \tilde{\phi} \star \tilde{\phi}$. Then $\psi^\star$ is a wavelet in Ω which has a non-negative Fourier transform with a zero of even multiplicity at the origin $p = 0$. Also, ϕ will be a scaling function which is associated with a wavelet ψ which is different from the wavelet $\psi^\star$. The scaling function ϕ has a positive Fourier transform by definition.

The Calderón-Mallat decomposition (2.26) may then be expressed in the form

$$h(t) = \frac{1}{C_{\tilde{\psi}}} \int_0^\sigma [W^\star h](s,t) \frac{ds}{s^2} + \frac{1}{C_{\tilde{\psi}}\sigma} [Vh](\sigma, t), \tag{2.27}$$

where

$$[W^\star h](s,t) = (h \star \psi_s^\star)(t), \tag{2.28}$$

$$[Vh](\sigma,t) = (h \star \phi_\sigma)(t), \tag{2.29}$$

and

$$\psi_s^\star = \frac{1}{\sqrt{s}} \tilde{\psi}_s \star \tilde{\psi}_s, \tag{2.30}$$

$$\phi_\sigma = \frac{1}{\sqrt{\sigma}} \tilde{\phi}_\sigma \star \tilde{\phi}_\sigma. \tag{2.31}$$

We are now in a position to make the connection between the Calderón-Mallat decomposition and the theory of linear viscoelasticity. Making the specific choice of scaling function

$$\phi(t) = \operatorname{sech}(t), \tag{2.32}$$

we can express equation (2.27) as

$$h(t) = \frac{1}{\pi} \int_0^1 \left(h \star \tilde{\psi}_s \star \tilde{\psi}_s\right)(t) \frac{ds}{s^2} + \frac{1}{\pi} g_2(t), \tag{2.33}$$

since it may be shown that $C_{\tilde{\psi}} = \pi$. In physical variables, this reads

$$H(\tau) = \frac{2}{\pi} G''\left(\tau^{-1}\right) + E(\tau), \tag{2.34}$$

where

$$E(\tau) = \frac{1}{\pi}\int_0^1 \left(h \star \tilde{\psi}_s \star \tilde{\psi}_s\right)(t)\,\frac{ds}{s^2}, \quad t = \ln\left(\tau^{-1}\right). \tag{2.35}$$

Clearly, $E(\tau)$ is the error term in the Fuoss and Kirkwood approximation (2.10).

Theorem 1: Let $h(t) \in L^2(\mathbb{R})$, i.e. let

$$\int_{-\infty}^{\infty} [H(\tau)]^2 d\ln\tau < \infty. \tag{2.36}$$

Then $E(\tau)$ is a wavelet in Ω^+ in the logarithmic variable $t = \ln\left(\tau^{-1}\right)$. Furthermore:

$$E(\tau) = \frac{1}{\pi}\int_0^1 \left(h \star \psi_s^\star\right)(t)\, s^{-3/2} ds, \tag{2.37}$$

with

$$\psi^\star(t) = \mathrm{sech}(t)\left[1 - t\tanh(t)\right]. \tag{2.38}$$

Proof. From (2.24) and (2.34), we have

$$E(\tau) = h(t) - \frac{1}{\pi}(h \star \phi)(t). \tag{2.39}$$

Hence the logarithmic Fourier transform is given by

$$\int_{-\infty}^{\infty} E(\tau) e^{-ipt} dt = \hat{h}(p)\left[1 - \frac{1}{\pi}\hat{\phi}(p)\right], \tag{2.40}$$

where $\hat{\phi}(p) = \pi\mathrm{sech}\left(\frac{1}{2}\pi p\right)$. To show that $E(\tau)$ is a wavelet in Ω^+, we must show that properties (2.12) and (2.13) are satisfied. Writing $p = 0$ in (2.40) we immediately see that

$$\int_{-\infty}^{\infty} E(\tau) dt = 0, \tag{2.41}$$

which satisfies (2.12). Finally, it can be seen that

$$\int_0^{\infty} |\hat{h}(p)|^2 \frac{|1 - \frac{1}{\pi}\widehat{\phi}(p)|^2}{p} dp < \infty, \tag{2.42}$$

since $p^{-1}\left[1 - \mathrm{sech}\left(\frac{1}{2}\pi p\right)\right]^2$ is bounded and $\int_{-\infty}^{\infty} |\hat{h}(p)|^2 dp < \infty$. That the wavelet $E(\tau)$ takes the form (2.35) follows from (2.33), where

$$\psi^\star(t) = \tilde{\psi}(t) \star \tilde{\psi}(t) = \frac{d}{dt}\left[t\tilde{\phi}(t) \star \tilde{\phi}(t)\right] = \frac{d}{dt}[t\mathrm{sech}(t)]. \tag{2.43}$$

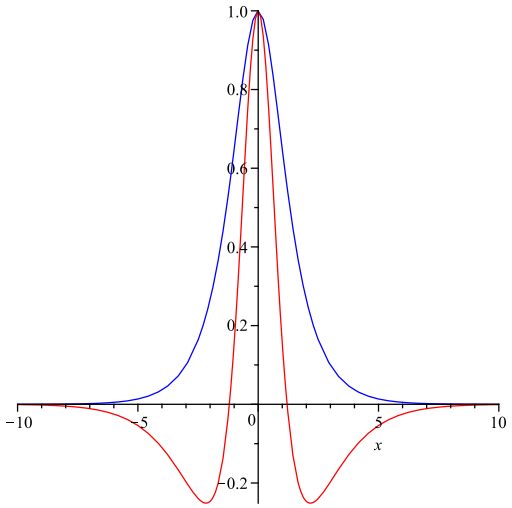

Figure 2: $\psi^\star(x)$ (—), $\phi(x)$ (—).

$(\psi^\star, \phi)$ are plotted together in Fig. 2.

The above theorem demonstrates, through the choice of hyperbolic scaling function $\phi(x)$ =sech(x), that there is a direct connection between the theory of linear viscoelasticity and continuous wavelet analysis. We now move on to the practical details of recovering $H(\tau)$ from the storage and loss moduli, by means of the inversion formula (2.27). Throughout the rest of the paper we restrict attention to the hyperbolic scaling function (2.32), which provides a natural dictionary from which a sparse approximation of the continuous spectrum can be selected.

3. Approximation and Regularization Strategy

3.1. Scale and sparsity as regularizers

Suppose that the relaxation spectrum $h(t)$ consists of a single peak of scale σ, e.g. the unimodal spectrum

$$H(\tau) = \frac{2\tau^2}{1+\tau^4} \tag{3.1}$$

may be written as $h(t) = \text{sech}(2t)$ with a scale of $\sigma = \frac{1}{2}$. The loss modulus may then be written as

$$g_2(x) = \int_{-\infty}^{\infty} \text{sech}(t) h(x-t) dt \approx \sum_k a_k h(x - ka), \tag{3.2}$$

where $a_k = a\ \text{sech}(ka)$ and $a > 0$ is a sampling rate. Since the loss modulus has a larger scale than that of $h(t)$, equation (3.2) demonstrates that a function

of larger scale may be expressed as the sum, with positive coefficients a_k, of translates of a function of a smaller scale. Furthermore, since

$$E(\tau) = h(t) - \frac{1}{\pi} g_2(t), \tag{3.3}$$

we deduce that a function containing scales smaller than σ may be expressed as a sum of translates of $h(t)$, where all but one of the coefficients are negative. Since $E(\tau)$ has zero area, we may deduce that

$$\sum_k a_k \approx \pi \quad \text{or} \quad \sum_k \operatorname{sech}(ka) \approx \frac{\pi}{a}. \tag{3.4}$$

The approximations in (3.2) and (3.4) can be made as accurate as we wish, by choosing a sufficiently small.

The above discussion is easily extended to spectra with more than one peak. As a possible basis for $h(t)$, consider the set of translated scaling functions

$$\phi_{\sigma,k}(t) \quad = \quad \phi\left(\frac{t - t_k}{\sigma}\right), \tag{3.5}$$

taken over all integers k, where

$$t_k = t_0 + k\mu, \tag{3.6}$$

μ is an integer multiple of the sampling rate a, and $\phi_{\sigma,0}$ is centred at t_0. This set spans a subspace V_σ of $L^2(\mathbb{R})$, whose resolution is governed by the scale parameter σ. The projection of $h(t)$ onto the subspace V_σ constitutes a regularized approximation $h_\sigma(t)$ to $h(t)$ of the form

$$h_\sigma(t) = \sum_k b_k \phi_{\sigma,k}(t). \tag{3.7}$$

$h_\sigma(t)$ contains projections from both parts of (2.27), and consequently contains negative components from the wavelet terms. This means that while $h_\sigma(t)$ should be positive for all t, the coefficients b_k themselves are not constrained to be positive.

The representation in (3.7) still offers an infinite number of degrees of freedom. In the field of sparse signal decomposition the set of functions

$$D = \{\phi_{\sigma,k}(t) : k \text{ an integer}; \sigma > 0, a > 0\} \tag{3.8}$$

is called a *redundant dictionary*, since only a few of its terms may be needed in determining a good approximation. Detailed reviews of wavelet dictionaries and their use can be found in [27,28]. Each element of the dictionary is called an *atom*. In this paper we will focus on constructing *m-sparse* approximations for the continuous relaxation spectrum $h(t)$ by selecting atoms from the dictionary for specific values of σ and a. When $0 < \sigma < 1$ then the m-sparse approximation takes the form

$$h_\sigma(t) = \sum_{k \in \Lambda_m} b_k \phi_{\sigma,k}(t), \tag{3.9}$$

where Λ_m is an index set with m entries. Sparsity is an important regularizer in its own right in the field of signal processing [27]. For example, sparsity is the sole criterion in the parsimonious approach advocated by Baumgaertel and Winter [8] in their recovery of discrete relaxation spectra.

3.2. Real-Time Integrability

Every viscoelastic material possesses a finite total viscosity. This imposes an integral constraint on $H(\tau)$ and $h(t)$, given by

$$\int_0^\infty H(\tau)d\tau = \int_{-\infty}^\infty h(t)e^{-t}dt < \infty. \tag{3.10}$$

We define any function $h \in L^2(\mathbb{R})$ which satisfies (3.10) to be *real-time integrable* (RTI). In particular, an atom in the dictionary D is RTI if

$$\int_{-\infty}^\infty \operatorname{sech}\left(\frac{t}{\sigma}\right) e^{-t}dt < \infty, \tag{3.11}$$

which is satisfied only when $0 < \sigma < 1$. For other values of σ, it is possible to combine three or more atoms in the dictionary to obtain a real-time integrable basis element. In particular, when $0 < \sigma < 3$ the three atoms $\phi_\sigma(t)$, $\phi_\sigma(t-b)$ and $\phi_\sigma(t+b)$, where b is a non-zero integer multiple of a, are configured into a triplet

$$\phi_\sigma^{[b]}(t) = \frac{\phi_\sigma(t) - \frac{1}{2}\phi_\sigma(b)\left\{\phi_\sigma(t-b) + \phi_\sigma(t+b)\right\}}{1 - \phi_\sigma^2(b)}. \tag{3.12}$$

The cancellation introduced by the negative terms in (3.12) means that the combination of all three terms decays like $e^{3t/\sigma}$ as $t \to -\infty$, and consequently is RTI.

It is easily shown that the basis element $\phi_\sigma^{[b]}(t)$, with $b \neq 0$, is positive for all values of t. Combinations of atoms of this kind can always be made so that the resulting basis is RTI for any positive value of σ.

3.3. Effective Bandwidth and Effective Bandlimit

Consider the gaussian function $e^{-\frac{1}{2}x^2/\sigma^2}$. Its scale is given by the standard deviation σ. It is well known that approximately 99.7% of the area under the curve is contained in the interval $[-3\sigma, 3\sigma]$. Since the Fourier transform of a gaussian is a gaussian with standard deviation σ^{-1}, then approximately 99.7% of the area of the Fourier transform is contained in the interval $[-3/\sigma, 3/\sigma]$. We may therefore define the *effective bandwidth* of the gaussian to be $6/\sigma$ and the *effective bandlimit* to be $3/\sigma$.

For a general function $h \in L^2(\mathbb{R})$, there is more than one way of defining an effective bandwidth. For consistency, however, we choose the same definition as we have taken for the gaussian, i.e. $h \in L^2(\mathbb{R})$ has an effective bandlimit β if approximately 99.7% of the area under the absolute value of its Fourier

transform is contained in the interval $[-\beta, \beta]$. A simple calculation reveals that we can conveniently attribute an effective bandlimit of $3.86/\sigma$ to an atom ϕ_σ in D. The unit of measurement is a reciprocal unit of natural log-frequency or a reciprocal unit of natural log-time.

In §3.2 we have shown that not all atoms in D are RTI. We therefore choose an alternative basis for V_0, for which each element is RTI. Such a basis is provided by atoms in the dictionary

$$D^+ = \left\{ \phi^{[b]}_{\sigma,k}(t) : k \text{ an integer}; 0 < \sigma < 3, 0 < a, 0 < b \leq \infty \right\}. \tag{3.13}$$

For $0 < \sigma < 3$, the atoms in D are also atoms of D^+, since $\phi_{\sigma,k} = \phi^{[\infty]}_{\sigma,k}$. However, the converse is not true, although with $b < \infty$ the atoms in D^+ are combinations of those in D. In the new basis, the approximation (3.9) is replaced by the m-sparse approximation

$$h_\sigma(t) = \sum_{k \in \Lambda_m} b_k \phi^{[b]}_{\sigma,k}(t). \tag{3.14}$$

In §3.1 we remarked that the resolution of the subspace V_0 is governed by the scale parameter σ. The dependence on σ of the resolution can now be quantified very precisely by the function $\beta(\sigma^{-1}b)$, where β is the effective bandlimit of an atom $\phi^{[b]}_\sigma$ in D^+. This function has been computed numerically for $\sigma = 1$ and is shown in Fig. 3. For general values of σ we deduce from the figure that

$$\frac{3.75}{\sigma} < \beta(\sigma^{-1}b) < \frac{5.81}{\sigma}. \tag{3.15}$$

The smallest bandlimit is attained when $b \simeq 1.44\sigma$ and the largest bandlimit is attained in the limit $b \to 0^+$. In the limit $b \to \infty$, it can be seen that $\beta \to 3.86/\sigma$. In particular, it can be shown that

$$\phi^{[0^+]}(t) = \operatorname{sech}^3(t) \quad \text{and} \quad \phi^{[\infty]}(t) = \operatorname{sech}(t). \tag{3.16}$$

In Fig. 4 is shown the shape of the atom $\phi^{[b]}_\sigma(t)$ for a range of values of b with $\sigma = 1$. We note that the width of each atom increases with b and, in consequence, the highest resolution is attained when $b = 0^+$, and the lowest when $b = \infty$. For practical purposes, the shape of the atom is unchanged when $b > 5$. Although the parameter b affects the resolving power of the atom, it does not affect the decay rate of $\phi^{[b]}_\sigma(t)$ as $b \to \pm\infty$. The decay rate of $\phi^{[b]}_\sigma(t)$ is $\operatorname{sech}(3t/\sigma)$, which is independent of the value of b. b should therefore be viewed as a tuning parameter, which fine-tunes the resolution at a fixed scale σ.

We have defined an effective bandlimit for any function $h \in L^2(\mathbb{R})$. Suppose that the effective bandlimit of the continuous spectrum h is β_h and the effective bandlimit of its approximation h_σ is β_{reg}. If $\beta_{reg} > \beta_h$, then the approximation h_σ exhibits *model-induced super-resolution*. If β_{reg} is significantly larger than β_h then super-resolution can result in a number of artificial peaks in the approximation. This is inherent in the case of a discrete spectrum, for which $\sigma = 0$ and $\beta_{reg} = \infty$. If $\beta_{reg} < \beta_h$, then the approximation to the spectrum is *under-resolved*.

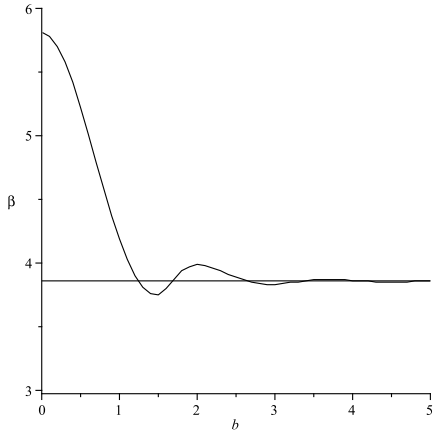

Figure 3: The bandlimit $\beta(b)$ of $\phi_\sigma^{[b]}$, as a function of b, when $\sigma = 1$.

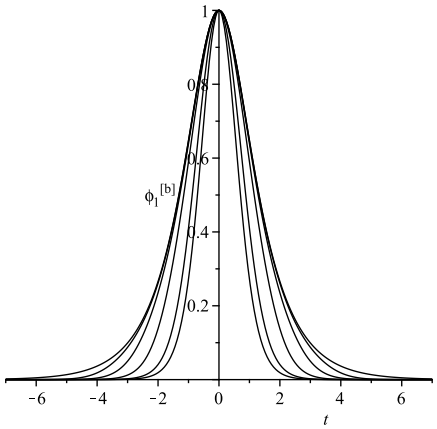

Figure 4: The atoms $\phi_1^{[b]}(t)$ for $b = 0^+, 1, 2, 3, 4$ and ∞.

3.4. Splitting the Atom: An Illustration of Discrete Calderón-Mallat Decomposition

A simple example of discrete Calderón-Mallat decomposition is afforded by splitting the atom

$$\phi_{1,0}^{[1]}(t) = \left(\frac{\alpha^2}{\alpha^2-1}\right)\phi(t) - \frac{1}{2}\left(\frac{\alpha}{\alpha^2-1}\right)\left[\phi(t-1)+\phi(t+1)\right], \tag{3.17}$$

where $\alpha = \cosh(1)$. With $h(t) = \phi_{1,0}^{[1]}(t)$, equation (2.9) gives the exact split

$$h(t) = \frac{1}{\pi}g_2(t) + E(\tau), \tag{3.18}$$

where $g_2(t) = \operatorname{sech}(t) \star \phi_{1,0}^{[1]}(t)$. As indicated in Section 2.3, equation (3.18) is an exact Calderón-Mallat decomposition of the continuous spectrum, and is shown in Fig. 5 (continuous lines). A discrete Calderón-Mallat decomposition is obtained by projecting in turn each of the two terms on the right of (3.18) onto the 3-dimensional subspace spanned by $\{\phi(t), \phi(t-1), \phi(t+1)\}$. A projection which preserves the total viscosity η and the total rigidity $G'(\infty)$ of the model is given by

$$\frac{1}{\pi}g_2(t) \approx c_0\phi(t) + c_1\phi(t-1) + c_1\phi(t+1), \tag{3.19}$$

where c_0 and c_1 are positive coefficients given by

$$c_0 = -\frac{\alpha}{(\alpha^2-1)}\left[1 + \frac{2\alpha(1-\alpha\beta)}{\pi\beta(\alpha-1)}\right], \tag{3.20}$$

$$c_1 = \frac{1}{2}\frac{\alpha^2}{(\alpha^2-1)}\left[1 + \frac{2(1-\alpha\beta)}{\pi\beta(\alpha-1)}\right], \tag{3.21}$$

where $\beta = \sinh(1)$, and

$$E(\tau) \approx c_2\left[\phi(t) - \tfrac{1}{2}(\phi(t-1)+\phi(t+1))\right], \tag{3.22}$$

where

$$c_2 = \frac{\alpha}{(\alpha-1)}\left[1 + \frac{2\alpha(1-\alpha\beta)}{\pi\beta(\alpha^2-1)}\right]. \tag{3.23}$$

The approximations (3.19) and (3.22) are depicted by the point symbols in Fig. 5. Although the individual approximations (3.19) and (3.22) are not RTI, the sum of the two is RTI. In Fig. 6 the Fourier transforms of these approximations is shown. Observe that in Fig. 5, the resolution afforded by the wavelet is greater than that of the loss modulus, while in Fig. 6 the wavelet is seen to provide the necessary effective bandwidth needed to recover the spectrum.

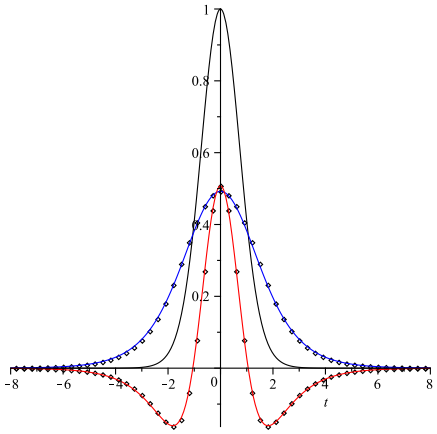

Figure 5: Splitting the atom $\phi^{[1]}_{1,0}(t)$ ($\sigma = 1, t_0 = 0$) into its constituent parts (3.18). On the scale of the figure, the approximations (3.19) and (3.22) (. . ., . . .) are indistinguishable from their exact counterparts (_, _).

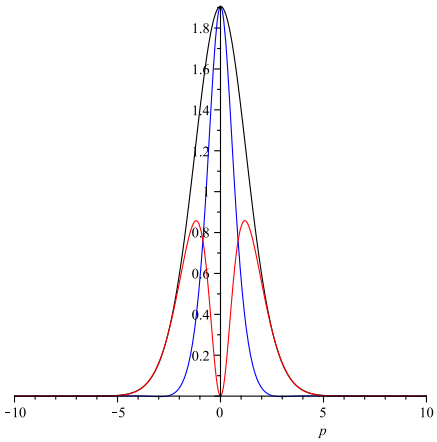

Figure 6: Splitting the atom $\phi^{[1]}_{1,0}(t)$ ($\sigma = 1, t_0 = 0$) in Fourier space.

4. Fitting the G', G'' Data

4.1. Transformed Dictionaries for G' and G''

We have seen that (3.14) provides a regularized model for the continuous relaxation spectrum in terms of atoms from the dictionary D^+. From equations (2.3) and (2.4), corresponding models for the storage and loss moduli are given by

$$G'(\omega) = g_1(x) = \sum_{k\in\Lambda_m} b_k \phi^{[b]}_{\sigma,k}(x) \star [1+\tanh(x)], \quad x = \ln\omega, \tag{4.1}$$

$$G''(\omega) = g_2(x) = \sum_{k\in\Lambda_m} b_k \phi^{[b]}_{\sigma,k}(x) \star \operatorname{sech}(x). \tag{4.2}$$

The convolution terms in (4.1) and (4.2) are the real and imaginary parts of complex atoms in the *transformed dictionary*

$$\begin{aligned} T^+ = \Big\{ & \phi^{[b]}_{\sigma,k}(x) \star [\operatorname{sech}(x) + i(1+\tanh(x))] : k \text{ an integer;} \\ & 0<\sigma<3, 0<a, 0<b\le\infty \Big\}. \end{aligned} \tag{4.3}$$

The atoms in T^+ are themselves combinations of simpler convolutions of the form

$$\phi_\sigma(x) \star [1+\tanh(x)] \quad \text{and} \quad \phi_\sigma(x) \star \operatorname{sech}(x). \tag{4.4}$$

For rational values of σ, the required convolutions can be evaluated in closed form using residue calculus. The resulting formulae for various values of σ are listed in Tables 1 and 2. In Fig. 7 we have plotted the convolutions (4.4) for $\sigma = \frac{1}{2}$.

σ	$\operatorname{sech}(\sigma^{-1}x) \star [1+\tanh(x)]$
2	$2\pi\left[1+\tanh(x) - \sqrt{2}\operatorname{sech}(x)\sinh\left(\frac{1}{2}x\right)\right]$
1	$\pi[1+\coth(x) - \operatorname{cosech}(x)] \quad (x\neq 0)$ $\pi \quad (x=0)$
1/2	$\frac{1}{2}\pi[1+\tanh(2x)] - 2x\operatorname{sech}(2x)$
1/4	$\frac{\pi}{4}\left(1+\operatorname{sech}(4x)\left[\sinh(4x) - 2\sqrt{2}\sinh(2x) + \frac{8}{\pi}x\right]\right)$

Table 1: Atoms in the transformed dictionary for G' data.

The coefficients b_k in (3.14) can now be determined by fitting the models (4.1) and (4.2) by weighted least-squares regression to measured values of G' and G''.

σ	$\mathrm{sech}(\sigma^{-1}x) \star \mathrm{sech}(x)$
2	$2\pi\mathrm{sech}(x)\left[\sqrt{2}\cosh\left(\frac{1}{2}x\right)-1\right]$
1	$2x\mathrm{cosech}(x) \quad (x \neq 0)$ $2 \quad (x=0)$
1/2	$\pi\mathrm{sech}(2x)[\sqrt{2}\cosh(x)-1]$
1/4	$\pi\mathrm{sech}(4x)\left[A\cosh(3x)-B\cosh(x)+1\right]$

Table 2: Atoms in the transformed dictionary for G'' data, where $A = \sqrt{1-1/\sqrt{2}}$ and $B = \sqrt{1+1/\sqrt{2}}$.

4.2. Search Algorithm

We assume that the available data $G'(\omega_j)$, $G''(\omega_j)$ are measured at N values of frequency ω_j, $j = 1, ..., N$. There are many choices of algorithm for fitting the data by constructing m-sparse approximations from atoms in a dictionary such as T^+. This is a rich area of research, known as *basis pursuit* [28,29]. For the purpose of this paper it is sufficient to use a simple search algorithm, which performs one regression per parameter selection on a 3-dimensional grid of parameters.

Let μ be a spacing parameter, which is an integer multiple of the sampling rate a. For a fixed parameter selection $\{\sigma, \mu, b\}$, only atoms in T^+ which are separated by log-frequency μ are selected. Typically, an initial 3-dimensional grid of parameters $\{\sigma, \mu, b\}$ will contain no more than 4^3 selections. Regressions are performed with selections from the grid for different values of m. The value of t_0 is initially selected so that there is a value of t_k close to a local maximum of $g_2(x)$. The value of t_0 is then refined as part of the search algorithm. In particular, the weighted sum of squared residuals

$$S = \sum_j \left[\frac{\Delta_1(x_j)}{G'(\omega_j)}\right]^2 + \sum_j \left[\frac{\Delta_2(x_j)}{G''(\omega_j)}\right]^2, \tag{4.5}$$

where

$$\Delta_1(x_j) = G'(\omega_j) - g_1(x_j), \tag{4.6}$$
$$\Delta_2(x_j) = G''(\omega_j) - g_2(x_j), \tag{4.7}$$

with $x_j = \ln \omega_j$ is minimized, and the root mean square error (RMS) evaluated:

$$\text{RMS error} = \sqrt{\frac{1}{2N}S} \times 100\%. \tag{4.8}$$

We compare the data fits and their associated spectra $h_R(t)$ for different values of m and σ, and select the smallest value of m compatible with acceptable RMS error levels.

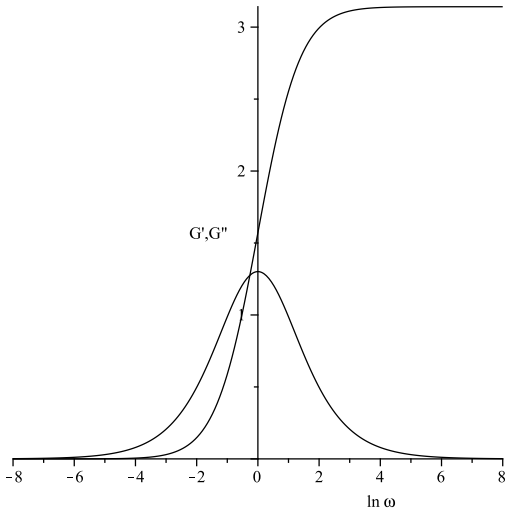

Figure 7: Scaling function convolutions from Tables 1 and 2 ($\sigma = \frac{1}{2}$).

5. Results and Discussion

In this section we reconstruct continuous relaxation spectra from both real and synthetic data. For the case of synthetic data, we use two separate double log-normal distributions, one of which is noise-free (DLN1) and one which has added noise (DLN2).

5.1. Double Log-Normal Spectrum Approximation

We first give an example of how well our models can fit synthetic data that do not contain any noise. The first example (DLN1), which was proposed by Stadler & Bailly [21], is the double log-normal spectrum

$$H(\tau) = h(t) = \sum_{k=0}^{1} a_k \exp\left[-\frac{1}{8}(t - t_k^\star)^2\right] \quad \left(t = \ln\left(\tau^{-1}\right)\right), \tag{5.1}$$

where the two peaks are centred at $t_0^\star = 4 - 3\ln 10 \approx -2.91$ and $t_1^\star = 4$, with equal heights $a_0 = a_1 = e^2/\left(2\sqrt{2\pi}\right) \approx 1.47$.

$G'(\omega)$ and $G''(\omega)$ are sampled at 33 values in the range $-8 \leq \ln\omega \leq 8$, with a sampling interval of 0.5. We approximate the spectrum as a sum of two atoms in the dictionary D^+. This approximation has the form

$$h_\sigma(t) \quad = \quad \sum_{k=0}^{1} b_k \phi_{\sigma,k}^{[b]}(t). \tag{5.2}$$

The storage and loss moduli are fitted with atoms from the transformed dictionary T^+, for values of σ given in Tables 1 and 2. With the second atom

centred at $t_1 = 4$, the search algorithm determines an optimal set of parameters $\sigma = 2$, $\mu = 6.9$, $b = 4$ and heights $b_0 = b_1 = 1.49$. With $m = 2$ the fit to the storage and loss moduli has an RMS error of 1.0%, and is shown in Fig. 8. The reconstructed spectrum is shown in Fig. 9 as a linear-log plot of $h(t)$ versus $-t$, which corresponds to a linear-linear plot of $H(\tau)$ against τ. This convention is used throughout the paper.

The effective bandlimit of the model (5.2) is $\beta_{reg} = 2$, while the effective bandlimit of the DLN1 spectrum is $\beta_h = 1.5$. It may be seen therefore that the search algorithm, which selects the model to minimize the RMS error (for a fixed value of m) does not necessarily select the model with least bandlimit. The reconstructed spectrum exhibits a very small amount of model-induced super-resolution. This is consistent with the observation that the peaks in the recovered spectrum are slightly higher and slightly narrower than the true spectrum [Fig. 9].

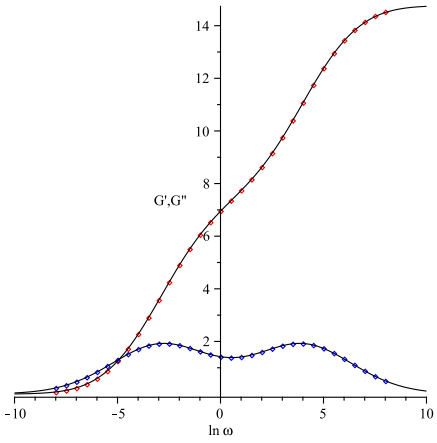

Figure 8: DLN1 data and fit with sech triplet reconstruction (equation 6.2).

Next we consider the double log-normal spectrum (DLN2) proposed by Honerkamp & Weese [10]. This is of the form

$$H(\tau) = h(t) = \sum_{k=0}^{1} a_k \exp\left[-\frac{1}{2}(t - t_k^\star)^2\right] \quad \left(t = \ln\left(\tau^{-1}\right)\right), \tag{5.3}$$

where the two peaks are centred at $t_0^\star = -\ln 5 \approx -1.61$ and $t_1^\star = \ln 20 \approx 3.00$, with equal heights $a_0 = a_1 = 1/\left(2\sqrt{2\pi}\right) \approx 0.20$.

Honerkamp & Weese provide $G'(\omega)$ and $G''(\omega)$ data at 30 values of ω in the range $-6.91 \leq \ln\omega \leq 6.91$, with a sampling interval of approximately 0.48. They add white noise with a standard deviation of 4% to the sampled values. To recover the spectrum we again use a two atom model of the form (5.2). Selecting transformed atoms from Tables 1 and 2, the search algorithm

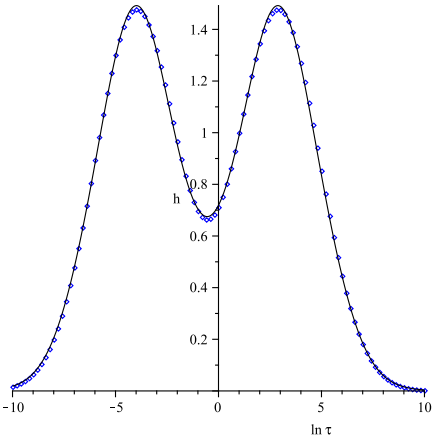

Figure 9: DLN1 spectrum (...). sech triplet reconstruction (___ (equation 6.2)).

determines an optimal set of parameters $\sigma = 1$, $\mu = 4.64$, $b = 1.75$, and heights $b_0 = 0.237$ and $b_1 = 0.238$, with the two atoms centred at $t_0 = -1.62$ and $t_1 = 3.02$. The fit to the storage and loss moduli has an RMS error of 5.1%, which is consistent with the noise level of 4% in the data. The data fit is shown in Fig. 10 and the reconstructed spectrum is shown in Fig. 11.

The effective bandlimit of the recovered spectrum is $\beta_{reg} \approx 3.9$, while the effective bandlimit of the DLN2 spectrum is $\beta_h = 3$. The reconstructed spectrum again exhibits a small amount of model-induced super-resolution, which is evident from Fig. 11. The amount of super-resolution as determined by the ratio β_{reg}/β_h is essentially the same in both cases. The recovered spectrum for DLN2, however, is less accurate due to the presence of noise.

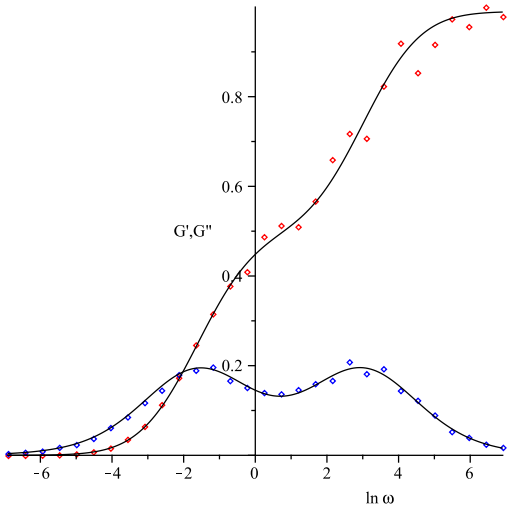

Figure 10: DLN2 data with two-atom fit.

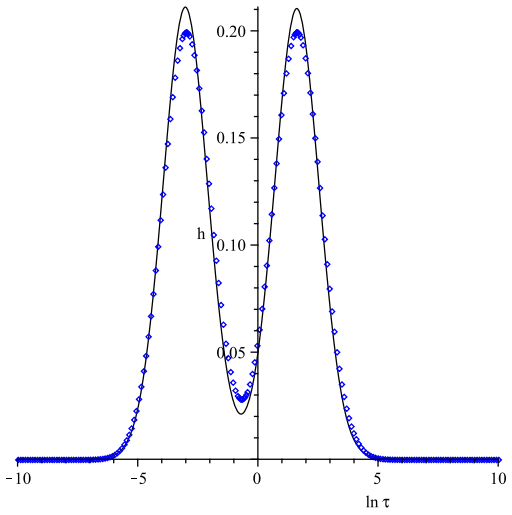

Figure 11: DLN2 spectrum (...). Two-atom reconstruction (___).

5.2. Real data

The recovery of the spectra in the synthetic cases DLN1 and DLN2 is relatively straight forward. There are two reasons for this. First, the range of the G', G'' data available is sufficient to determine the whole spectrum, i.e. the data sets in each case are essentially complete. Secondly, the clear bimodal shape of $g_2(x) = G''(\omega)$ makes it relatively easy to determine the scale of the atoms chosen from the transformed dictionary. When dealing with real data the situation need not be so straight forward. For real data the range of frequencies is limited and the shape of G'' may not give any clues as to the shape of the spectrum.

In our third and final example we compare the results from wavelet regularization with a spectrum recovered from real data by Honerkamp & Weese [10] using Tikhonov regularization. The data in question correspond to a polybutadiene polymer blend, which we denote by PBD1.

For this set of data the level of noise is not known. To achieve an RMS error of less than 5% for a range of scales $0 \leq \sigma < 2$, the least value of m required by the search algorithm is $m = 4$. To obtain an RMS error level less than 2% we require $\sigma < 1$. This leads to an estimate for the continuous relaxation spectrum of the form

$$h_\sigma(t) \quad = \quad \sum_{k=0}^{3} b_k \phi_{\sigma,k}(t) \quad (b = \infty). \tag{5.4}$$

For this m-sparse approximation, the parameter values which minimize the RMS error for different values of σ are given in Table 3, and the fits to the data together with their recovered spectra are shown in Figs. 12-15, for $\sigma = \frac{1}{2}$, $\frac{1}{3}$, $\frac{1}{6}$ and 0, respectively. With $\sigma > \frac{1}{2}$, our search algorithm failed to identify a positive sparse approximation which fitted the data to a tolerance of less than 2%. It is not obvious from these results what is the optimal choice of scale σ. Given that the amount of super-resolution increases with decreasing σ, however, a comparison of Figs. 12 and 13 would suggest that super-resolution sets in for a value of σ in the range $\frac{1}{3} < \sigma < \frac{1}{2}$. The recovered spectra in Figs. 12-15 differ significantly in shape: the number of peaks in the spectra vary from 2 to 4, depending on the value of σ. Furthermore, each recovered spectrum gives rise to models of storage and loss moduli (equations (4.1) and (4.2)) which fit the data to an acceptable tolerance. From the point of view of fitting the data, there is very little to distinguish between the spectra. Sparsity alone ($m = 4$) clearly cannot determine the shape of the spectrum: an additional criterion is required for choosing the scale σ.

Tikhonov and entropy regularization induce smoothness in the recovered spectrum by imposing penalty constraints. Such penalties are essentially *a priori* mechanisms for regularization. In implementing wavelet regularization, it is convenient to use instead an *a posteriori* criterion based on *minimum total curvature.*

σ	t_0	μ	b_0	b_1	b_2	b_3	RMS error (%)
1/2	2.95	1.20	-0.57	6.14	-1.92	3.87	2.0
1/3	2.47	1.52	-0.10	6.23	1.54	3.71	1.6
1/4	2.20	1.72	-0.02	7.69	3.48	4.36	1.4
1/6	3.77	1.27	9.47	5.08	3.41	5.56	1.2
1/7	3.73	1.23	10.48	6.26	3.54	6.77	1.3
0	3.61	1.16	3.96	3.34	1.12	3.34	1.4

Table 3: Parameter values which minimize the RMS error for different values of σ ($m = 4$). The b_k should be multiplied by 10^5 for their true value.

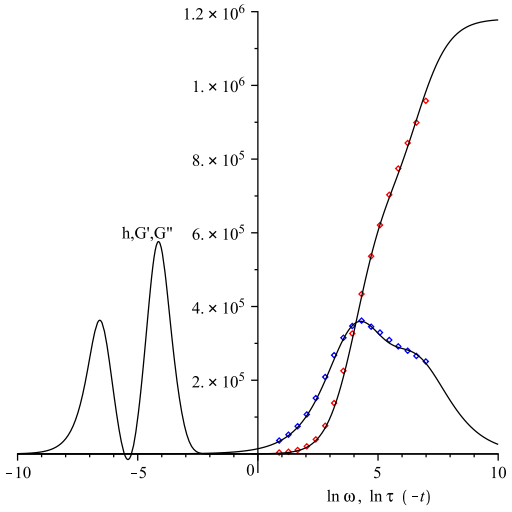

Figure 12: PBD1 data and fit. Sub-optimal 4-mode continuous spectrum. $\sigma = \frac{1}{2}$, RMS error=2.0%.

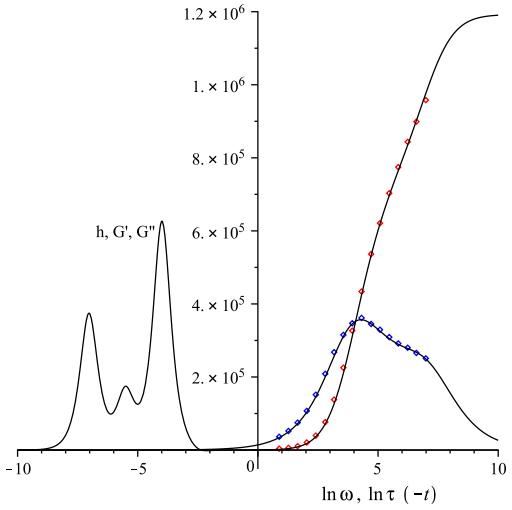

Figure 13: PBD1 data and fit. Super-resolved 4-mode continuous spectrum. $\sigma = \frac{1}{3}$, RMS error=1.6%.

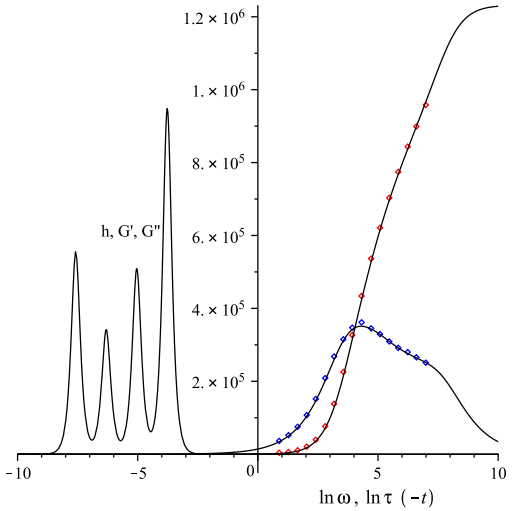

Figure 14: PBD1 data and fit. Super-resolved 4-mode continuous spectrum. $\sigma = \frac{1}{6}$, RMS error=1.2%.

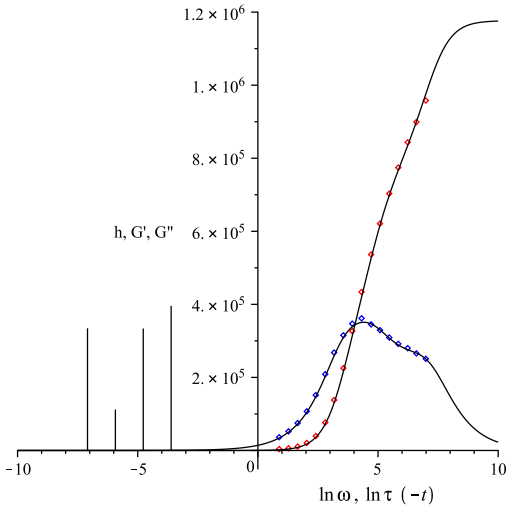

Figure 15: PBD1 data and fit. 4-mode discrete spectrum ($\sigma = 0$). RMS error=1.4%.

5.2.1. Minimum total curvature as a method for choosing σ.

Starting with the premise that spectra are necessarily smooth, we choose the smallest value of m and a value of σ which together give the smoothest spectrum that fits the data to an acceptable tolerance. An examination of Fig's 12-15 would suggest that an acceptable tolerance in the PBD1 data would be an RMS error between 1% and 2%. The criterion of minimum total curvature normally determines the spectrum with the smallest number of peaks that gives an acceptable fit to the data.

The curvature, $k_\sigma(t)$, of a spectrum $h_\sigma(t)$ at the point t is given by

$$k_\sigma(t) \quad = \quad \frac{|h''_\sigma(t)|}{(1+[h'_\sigma(t)]^2)^{3/2}} \tag{5.5}$$

and the total curvature of the spectrum, T_σ, is given by

$$T_\sigma \quad = \quad \int_{-\infty}^{\infty} k_\sigma(t)dt. \tag{5.6}$$

T_σ is readily evaluated for any value of σ, and it is easily found that T_σ is minimized for a value σ in the range $\frac{1}{3} < \sigma < \frac{1}{2}$.

To allow interpolation between the values of $\sigma = \frac{1}{2}$ and $\sigma = \frac{1}{3}$ we define a linear homotopic approximation

$$h^+_\sigma \quad = \quad 3(1-2\sigma)h_\sigma|_{\sigma=\frac{1}{3}} + 2(3\sigma-1)h_\sigma|_{\sigma=\frac{1}{2}}, \tag{5.7}$$

and minimize T_σ as a function of σ in this range.

T_σ is minimized when $\sigma = 0.45$. For this value of σ the recovered spectrum determined by (5.7) and the corresponding storage and loss moduli are shown in Fig. 16. The RMS error in fitting the data is 1.8%.

In Fig. 17, the recovered spectrum with $\sigma = 0.45$ is normalized and compared with the normalized spectrum obtained by Honerkamp & Weese [10] using Tikhonov regularization. The vertical lines denote the error bars in the Honerkamp & Weese spectrum. The overall shapes of the two recovered spectra are consistent. The peaks in the homotopic approximation are centred at $\tau_a = 1.2 \times 10^{-3}$ and $\tau_b = 1.7 \times 10^{-2}$, while those obtained by Honerkamp & Weese are $\tau_a = 8 \times 10^{-4}$ and $\tau_b = 2 \times 10^{-2}$. The negative lobes appearing in the Honerkamp & Weese spectrum are a consequence of the Tikhonov filter, which results in an abrupt cut-off in the SVD. The hyperbolic filter inherent in the homotopic approximation has a much gentler rate of decay.

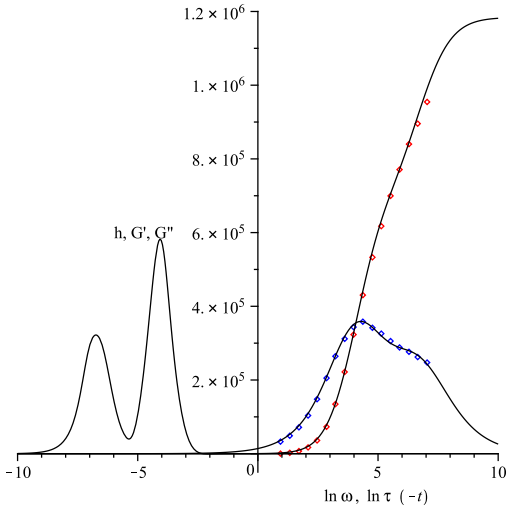

Figure 16: PBD1 data and fit. Optimal homotopic approximation via minimum total curvature criterion. $\sigma = 0.45$, RMS error=1.8%.

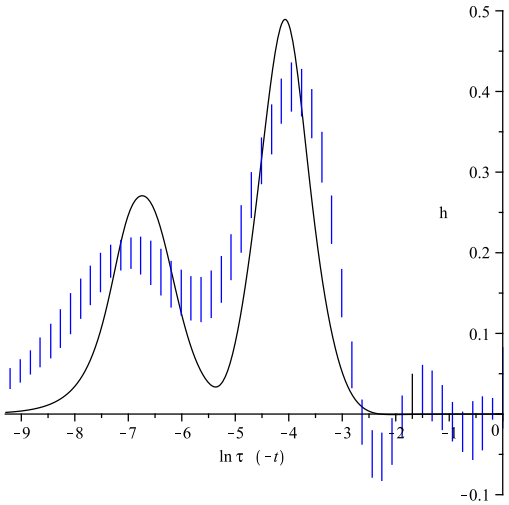

Figure 17: PBD1. Normalized homotopic spectrum obtained via minimum total curvature (——); Honerkamp & Weese spectrum (|||).

6. Conclusions

In this paper we have presented a dictionary of hyperbolic scaling functions for representing the continuous spectrum, together with its transformed dictionary of convolutions for representing the corresponding storage and loss moduli. Sparsity and scale are used as key parameters in constructing the spectrum, and the criterion of minimum total curvature is used to select an appropriate scale parameter σ.

The problem of recovering continuous spectra from storage and loss moduli is exponentially ill-posed. In consequence, there are a vast range of models of different shapes and parameterizations which can fit the dynamic data equally well over a limited range of measured frequencies. For example, all five models shown in Figs 12-16 reproduce the dynamic data to within an accuracy of 1.2% to 2.0%, yet they display a varying number of peaks and different distributions of concentration of viscosity. There is extreme sensitivity in the shape of the spectra to small changes in the parametrization.

It can be deduced from equation (2.4) and the analysis of §3.3 that the effective bandlimit of the loss modulus of any viscoelastic material cannot exceed 3.86 units of reciprocal log-frequency. On the other hand, there need be no limit on the effective bandlimit of any noise in the dynamic data. The effective bandlimit of an atom in the dictionary D is inversely proportional to the scale parameter σ, while the effective bandlimit of an atom in the transformed dictionary is inversely proportional to $\sigma + 1$. The smaller the value of σ then the

greater the capacity for fitting noise in the data. The smoother the spectrum then the greater the value of σ and the capacity for fitting the noise is reduced.

Given the extreme sensitivity of shape to parametrization, it is crucial that other tests and observations are used to impart confidence in the predicted approximate spectrum. In particular, if the spectrum is accurate in a limited range of relaxation times then G' and G'' must be accurate over a range of frequencies larger than the reciprocal range of the spectrum. This is an immediate consequence of the sampling localization demanded by equation (1.11).

In Fig. 16 we may infer from (1.11) that for frequencies in the range $0.9 < \ln\omega < 9.0$, the spectrum is determined in the range of relaxation times $-5.5 < \ln\tau < -2.5$. This tells us that we may place confidence in the higher peak but not in the lower. Confidence in the existence of the second peak would require a knowledge that the extrapolated dynamic data were accurate in the range $-0.7 < \ln\omega < 10.6$.

It is interesting in this context to examine the variation in the predicted plateau modulus $G'(\infty)$. When $0 < \sigma < \frac{1}{6}$ then the predicted value of $G'(\infty)$ varies between 1.177×10^6 and 1.232×10^6, a variation of almost 5%. When $\frac{1}{6} < \sigma < \frac{1}{3}$ then the predicted value of $G'(\infty)$ varies between 1.192×10^6 and 1.232×10^6, a variation of over 3%. When $\frac{1}{3} < \sigma < \frac{1}{2}$ then the predicted value of $G'(\infty)$ varies between 1.181×10^6 and 1.192×10^6, a variation of under 1%. These observations are entirely consistent with our earlier conclusion that the greater the value of σ the capacity for fitting noise in the data is reduced.

Acknowledgments

During the course of this research the second author was financially supported by EPSRC. The final stages of the work was completed whilst the first author was on study leave at the Isaac Newton Institute for Mathematical Sciences at Cambridge. The support from both institutions is gratefully acknowledged.

References

1. Boltzmann L (1874). Sitzb Kgl Akad Wiess Wien 2 (Abt 70):725
2. Saut JC, Joseph DD (1983). *Fading memory.* Arch. Rational. Mech. Anal. 81:53-95.
3. Bernstein SN (1928). *Sur les fonctions absolument monotones.* Acta Mathematica 52: 166.
4. Tanner RI, Walters K (1998). *Rheology: An Historical Perspective.* Elsevier, Amsterdam.
5. Walters K (1975). *Rheometry.* Chapman and Hall, London.
6. Davies AR , Anderssen RS (1997). *Sampling Localization in Determining the Relaxation Spectrum.* J. Non-Newtonian Fluid Mech. 73:163-179.
7. Renardy M (2008). *On the use of Laplace transform inversion for reconstruction of relaxation spectra* J. Non-Newtonian Fluid Mech. 154 (2008), pp. 47-51.

8. Baumgaertel M, Winter HH (1989). *Determination of Discrete Relaxation and Retardation Time Spectra from Dynamic Mechanical Data.* Rheol Acta 28:511-519.
9. Mustapha SMFDS, Phillips TN (2000). *A dynamic nonlinear regression method for the determination of the discrete relaxation spectrum.* Journal Of Physics D-Applied Physics 33:1219-1229.
10. Honerkamp J, Weese J (1989). *Determination of the relaxation spectrum by a regularization method.* Macromolecules 22:4372-4377.
11. Elster C, Honerkamp J (1992). *The role of the error model in the determination of the relaxation-time spectrum.* J Rheol 36:911-927.
12. Anderssen RS, Davies AR (2001). *Simple moving-average formulae for the direct recovery of the relaxation spectrum.* J Rheol 45:1-27.
13. Macdonald JR (2000). *On relaxation-spectrum estimation for decades of data: accuracy and sampling-localization considerations.* Inverse Problems 16:1561-1583.
14. Carrot C, Verney V (1996). *Determination of a discrete relaxation spectrum from dynamic experimental data using the Pade-Laplace method.* European Polymer Journal 32:69-77.
15. Malkin A.Ya. (2002). *The sense of a relaxation spectrum and methods for its calculation.* Vysokomol. Soedin. (Polymers in Russian) 44:1698-2005.
16. Chow MK, Zukoski CF (1995). *Gap size and shear history dependencies in shear thickening of a suspension ordered at rest.* J Rheol 39:15-32.
17. Chow MK, Zukoski CF (1995). *Nonequilibrium behavior of dense suspensions of uniform particles - volume fraction and size dependence of rheology and microstructure.* J Rheol 39:33-59.
18. Dealy JM, Larson RG (2006). *Structure and Rheology of Molten Polymers.* Hanser Gardner Publications, Cincinnati, Ohio.
19. Baumgaertel M, Winter HH (1992). *Interrelation between continuous and discrete relaxation time spectra.* J Non-Newton Fluid Mech 44:15-36.
20. Anderssen RS, Saiful A Husain (2005). *Modelling the relaxation modulus of linear viscoelasticity using Kohlrausch functions.* J Non-Newton Fluid Mech 125:159-170.
21. Stadler FJ, Bailly C (2009). *A new method for the calculation of continuous relaxation spectra from dynamic-mechanical data.* Rheol Acta 48:33-49.
22. Stadler F (2010). *Effect of incomplete datasets on the calculation of continuous relaxation spectra from dynamic-mechanical data* Rheol Acta 49:1041-1057.
23. Malkin A Ya (2006). *The use of a continuous relaxation spectrum for describing the viscoelastic properties of polymers.* Polymer Science Series A 48:39-45.
24. Ferry JD (1980). *Viscoelastic properties of polymers.* Wiley, New York.
25. Fuoss R, Kirkwood J (1941). *Electrical Properties of Solids. VIII. Dipole Moments in Polyvinyl Chloride-Diphenyl Systems.* J Amer Chem Soc. 63:385-394.

26. Calderón AP (1964). *Intermediate spaces and interpolation, the complex method.* Stud. Math., 24:113-190.
27. Mallat S (2009). *A Wavelet Tour of Signal Processing. The Sparse Way.* Academic Press, San Diego, USA.
28. Chen SS, Donoho DL, Saunders MA (2001). *Atomic decomposition by basis pursuit.* SIAM Rev., 43:129-159.
29. Donoho DL, Elad M (2004). *On the stability of the basis pursuit in the presence of noise .* Signal Processing, 86(3):511-532.